Behavioral/Cognitive

The neural dynamics of novel scene imagery

Daniel N. Barry, Gareth R. Barnes, Ian A. Clark, and Eleanor A. Maguire*
Wellcome Centre for Human Neuroimaging, Queen Square Institute of Neurology,
University College London, London WC1N 3AR

***Corresponding author:** Wellcome Centre for Human Neuroimaging, Queen Square Institute of Neurology, University College London, 12 Queen Square, London WC1N 3AR, UK
T: +44-20-34484362; F: +44-20-78131445; E: e.maguire@ucl.ac.uk

Abbreviated title: Neural dynamics of scene imagery

Number of pages: 32
Number of figures: 6
Number of tables: 3
Abstract word count: 250
Significance statement word count: 120
Introduction word count: 648
Discussion word count: 1499

Acknowledgements: This work was supported by a Wellcome Principal Research Fellowship to E.A.M. (210567/Z/18/Z) and the Centre by a Centre Award from Wellcome (203147/Z/16/Z). The authors are grateful to David Bradbury for technical assistance.

The authors declare no competing financial interests.

Abstract

Retrieval of long-term episodic memories is characterised by synchronised neural activity between hippocampus and ventromedial prefrontal cortex (vmPFC), with additional evidence that vmPFC activity leads that of the hippocampus. It has been proposed that the mental generation of scene imagery is a crucial component of episodic memory processing. If this is the case, then a comparable interaction between the two brain regions should exist during the construction of novel scene imagery. To address this question, we leveraged the high temporal resolution of magnetoencephalography (MEG) to investigate the construction of novel mental imagery. We tasked male and female humans with imagining scenes and single isolated objects in response to one-word cues. We performed source level power, coherence and causality analyses to characterise the underlying inter-regional interactions. Both scene and object imagination resulted in theta power changes in the anterior hippocampus. However, higher theta coherence was observed between the hippocampus and vmPFC in the scene compared to the object condition. This inter-regional theta coherence also predicted whether or not imagined scenes were subsequently remembered. Dynamic causal modelling of this interaction revealed that vmPFC drove activity in hippocampus during novel scene construction. Additionally, theta power changes in the vmPFC preceded those observed in the hippocampus. These results constitute the first evidence in humans that episodic memory retrieval and scene imagination rely on similar vmPFC-hippocampus neural dynamics. Furthermore, they provide support for theories emphasising similarities between both cognitive processes, and perspectives that propose the vmPFC guides the construction of context-relevant representations in the hippocampus.

Significance statement

Episodic memory retrieval is characterised by a dialogue between hippocampus and ventromedial prefrontal cortex (vmPFC). It has been proposed that the mental generation of scene imagery is a crucial component of episodic memory processing. An ensuing prediction would be of a comparable interaction between the two brain regions during the construction of novel scene imagery. Here, we leveraged the high temporal resolution of magnetoencephalography (MEG), and combined it with a scene imagination task. We found that a hippocampal-vmPFC dialogue existed, and that it took the form of vmPFC driving the hippocampus. We conclude that episodic memory and scene imagination share fundamental neural dynamics, and the process of constructing vivid, spatially coherent, contextually appropriate scene imagery is strongly modulated by vmPFC.

Introduction

Episodic memory formation and retrieval are long-established functions of the hippocampus (Scoville and Milner, 1957). However, cognitive impairments beyond recalling past experiences have been documented following hippocampal damage, including deficits in imagination and future-thinking (Hassabis et al., 2007a; Kwan et al., 2010; Kurczek et al., 2015). Accordingly, contemporary perspectives have converged on a more inclusive account of hippocampal function which accommodates the flexible construction of predictive or fictive representations (Hassabis and Maguire, 2007; Schacter and Addis, 2007; Eichenbaum and Fortin, 2009; Buckner, 2010; Maguire and Mullally, 2013).

One such interpretation, the Scene Construction Theory, proposes that the hippocampus constructs scene imagery to facilitate mental representations, whether recollected or imagined (Hassabis and Maguire, 2007; Maguire and Mullally, 2013). In this context, a scene is defined as a naturalistic three-dimensional spatially-coherent representation of the world typically populated by objects and viewed from an egocentric perspective (Maguire and Mullally, 2013; Dalton et al., 2018). In support of this thesis, functional MRI (fMRI) studies have revealed particularly anterior hippocampal recruitment while participants imagined novel scenes (Hassabis et al., 2007b; Zeidman et al., 2015; Zeidman and Maguire, 2016).

However, other regions, including the ventromedial prefrontal cortex (vmPFC), are recruited during (Hassabis et al., 2007b), and seem necessary for (Bertossi et al., 2016a), scene construction. An outstanding question, therefore, is how vmPFC interacts with hippocampus during the generation of scene imagery. The temporal resolution of magnetoencephalography (MEG) renders it a suitable method to address this question. Furthermore, a proposed mechanism of such inter-regional communication is oscillatory coherence (Fries, 2005). Increased theta synchrony between hippocampus and vmPFC has been observed during episodic memory retrieval (Fuentemilla et al.,

2014) and integration (Backus et al., 2016), as well as memory-guided navigation (Kaplan et al., 2014) and decision-making (Guitart-Masip et al., 2013). Demonstrating analogous connectivity during the imagination of novel scenes would provide evidence that episodic memory and scene construction share not only similar loci of brain activity, but are supported by comparable network dynamics.

If oscillatory coherence between hippocampus and vmPFC is evident during scene construction, a question of further relevance concerns the direction of information flow between the two regions. Electrophysiological investigations in rodents have suggested that during initial contextual memory formation, hippocampal activation precedes that of vmPFC (Place et al., 2016). By contrast, retrieval (Place et al., 2016), detection of violations in learned information in humans (Garrido et al., 2015) and subsequent extinction, have been characterised by vmPFC driving hippocampus. It is unclear which pattern the generation of novel scene imagery might follow.

Campbell et al. (2018) investigated the directionality of information flow between hippocampus and vmPFC during the imagination of future events using dynamic causal modelling (DCM; Friston et al., 2003) of fMRI data. This revealed a greater influence of hippocampus over vmPFC. However, the temporal resolution of fMRI is not optimal to adequately characterise this dialogue. In contrast, McCormick et al. (2018) recently proposed that vmPFC initiates scene construction. From this perspective, the vmPFC would drive the hippocampus during the imagination of novel scenes.

The current study, we leveraged the high temporal resolution of MEG to address two questions. First, do the anterior hippocampus and vmPFC display coherent activity during the imagination of novel scenes relative to single objects? Given accumulating evidence that theta oscillations mediate the interaction between hippocampus and vmPFC, we predicted greater theta coherence between the two regions specifically for scene imagery. Second, does one of these regions exert a stronger

influence over the other during scene imagination? Concordant with McCormick et al.'s (2018) proposal, we hypothesised that vmPFC would drive oscillatory activity in hippocampus. We asked participants to imagine novel scenes (and single isolated objects as a control condition) in response to single-word cues during MEG. A low-level baseline condition involving counting was also included. We then used a combination of source localisation techniques measuring power and coherence, as well as DCM for MEG to address the research questions.

Materials and Methods

Participants

Twenty-two participants (14 female) took part in this experiment (mean age 27 years; SD 7). Due to the verbal nature of the stimuli, only native English speakers were recruited. Participants gave written informed consent. The University College London Research Ethics Committee approved the study.

Stimuli

Seventy-five scene words and 75 object words were used as stimuli for the imagination task. These comprised a sub-set of the stimuli devised by Clark et al. (2018) for a separate fMRI study. These word categories were closely matched on a number of properties (Table 1) to ensure any differences in neural activity could be solely attributed to the type of mental imagery they evoked. To enable vivid imagination, all words were rated as highly imageable (> 3.5/5). To facilitate the ease with which participants could construct the two different kinds of representations, words were designated as either scene or object-evoking if at least 70% of an independent sample of participants rated them as such (Clark et al., 2018). Object imagery was included as a suitable control condition for scene imagery, as vivid detailed mental imagery can be evoked and viewed from an egocentric perspective, without the requirement to construct a three-dimensional space. Furthermore, object imagery has been used as a closely matched control for scene imagery in

153 previous neuroimaging studies (Clark et al., 2018; Hassabis et al., 2007b; Zeidman et al., 2015).
154 Additionally, 75 number stimuli were also deployed in a third condition involving counting, which
155 were matched to the scene and object words in terms of the number of letters and syllables. This
156 condition served as a useful low-level baseline against which to compare the neural activity common
157 to both scene and object imagery. Counting was preferred to a resting baseline, as such passive
158 states have been associated with spontaneous neural activity in our regions of interest (Vincent et
159 al., 2006).
160
161 **Experimental design of the task**
162 Prior to the MEG scan, participants received task instructions and practiced for the equivalent of two
163 in-scanner sessions. For the scene imagination task, the instructions were as follows: "You will hear a
164 word which evokes the mental image of a three dimensional space which you could step into, such
165 as "jungle". Then I want you to create as detailed a scene as you possibly can in your mind's eye. I
166 don't want you to recall something from memory, such as when you visited such a place before.
167 Instead, I want you to create the scene in your imagination. You will have just three seconds to do
168 this, so please try and let it come as quickly and naturally as possible, and hold this image in your
169 mind for the remainder of the three seconds". For the object imagination task, participants were
170 instructed to do the following upon presentation of an object word (e.g. "cushion"): "I want you to
171 imagine a single object against a white background, as if it is floating in space. There should be
172 nothing other than that object in your mind's eye, so no background or anything associated with it;
173 only the object. Also, try and make the object as large as possible, so that it takes up your entire field
174 of view." The counting baseline instructions were as follows: "count in threes from the presented
175 number" (e.g. "forty"). In the MEG scanner, experimental stimuli were delivered aurally via MEG-
176 compatible earbuds using the Cogent toolbox (www.vislab.ucl.ac.uk/cogent.php), running in
177 MATLAB (version 2012).
178

To prepare them for each trial type, participants first heard either the word “scene”, “object” or “counting” (Figure 1). This was intended to minimise category confusion during the scene and object trials. Participants immediately closed their eyes and waited for an auditory cue which followed a jittered duration of between 1300 and 1700 milliseconds. As previously detailed in the instructions to participants, during scene trials participants constructed a novel, vivid scene from their imagination. During object imagery, participants imagined a single novel object, and counting trials involved mentally counting in threes from a number cue. The task periods were 3000 ms in duration. Participants then heard a beep and opened their eyes. They were presented with a rating screen. For scene and object trials, they were asked “What did you imagine?” If they failed to perform the task, they selected “unsuccessful”. Otherwise, they could select “low detail scene”, “high detail scene”, “low detail object” or “high detail object”. This allowed participants to indicate both the level of detail present in the mental imagery, and also to reclassify scene and object trials if they had inadvertently imagined an object as a scene or vice versa. For counting trials, participants were asked “How well did you concentrate?” on a scale from 1 (not at all) to 5 (extremely well). Following this was a 1000 ms delay before the next trial. There were eight scanner sessions in total, seven containing nine stimuli from each condition in a random order, and one final session with 12 stimuli from each condition. Most sessions contained 27 trials as this corresponded to the optimal time that participants could comfortably remain still and concentrate, which resulted in an excess of three trials per condition for the final session. Eighteen participants completed all eight sessions; the remaining four participants completed seven sessions due to technical issues with the recording equipment.

Post-scan recognition memory test

After the scan, participants took part in a recognition memory test. Participants were not informed about this test prior to the scan to avoid confounding the imagination task with attempts to memorise the stimuli. They were presented with scene and object words, and asked if the word was

205 previously presented in the scanner or not. The available response options were “yes” or “no”.
206 Alongside the 75 scene and 75 object words which had been presented in the scanner, there were
207 38 scene and 38 object foils; the presentation was randomised for each participant. The scene and
208 object foil words were also matched to the words presented in the scanner on the characteristics
209 outlined in Table 1.
210
211 **Statistical analysis: behavioural data**
212 ***Word properties***
213 Comparisons between word category properties were performed using independent sample t-tests
214 in the case of continuous variables and chi squared tests for categorical variables. Significance was
215 determined at an alpha level of $p < 0.05$. Statistical analyses were performed using SPSS statistical
216 package version 22 (SPSS, Chicago, IL).
217
218 ***In-scanner ratings***
219 Comparison of the percentage of successful trials in each condition was performed using a repeated-
220 measures one-way ANOVA. These percentages accommodate participants’ reclassifications of
221 scenes and objects during task performance. Greenhouse–Geisser adjustment to the degrees of
222 freedom was applied if Mauchly’s sphericity test detected a violation of sphericity. Comparison of
223 trial reclassifications, and highly detailed ratings were performed using paired samples t-tests.
224
225 ***Post-scan recognition memory test***
226 To ensure a relevant comparison with trials used in the MEG analysis, only successfully completed
227 trials in the scanner were included as target stimuli in this analysis, and stimuli were reclassified as
228 scenes or objects if the individual participant had imagined them as such during the task.
229 Comparison of the percentage of correctly recognised scenes and objects, d’ and c (response bias)
230 values were performed using paired samples t-tests.

MEG recording and preprocessing

A CTF Omega whole-head MEG system with 273 functioning first order gradiometers recorded data at a sample rate of 1200Hz. Four EOG electrodes were used to measure a participant's vertical and horizontal eye movements. To rule out the possibility that differences between conditions in subsequent analyses were related to differences in eye movements, we computed the variance of these two EOG signals during each trial, which served as an indirect measure of saccadic activity. These variances were averaged across trials within each condition and normalised within subjects so that values for the three conditions summed to 1. A 1x3 repeated measures ANOVA did not detect any differences in eye movements between conditions ($F_{(2,42)} = 1.12$, $p = 0.335$). Data were epoched into 3 second mental imagery and counting periods, baseline corrected, and concatenated across sessions. For gamma (31-85 Hz) band analysis, a 50 Hz stop-band filter was applied to remove power line noise.

Statistical analysis: MEG data

All MEG analyses were performed using SPM12 (www.fil.ion.ucl.ac.uk/spm). Source reconstruction was performed using the SPM DAiSS toolbox (https://github.com/spm/DAiSS).

MEG source reconstruction

To estimate differences in power between experimental conditions in source space, the Linearly Constrained Minimum Variance (LCMV) beamformer was used. This filter uses a series of weights to linearly map MEG sensor data into source space to estimate power at a particular location, while attenuating activity from other sources. For each participant, a single set of filter weights was constructed based on the data from all three conditions within the 4-8 Hz band and a 0-3000 ms peri-stimulus window. Analysis was performed in MNI space using a 5 mm grid and coregistration was based on nasion, left and right preauricular fiducials. Co-registration and the forward model

were computed using a single-shell head model (Nolte, 2003). Power was estimated in the theta (4-8 Hz) frequency band and the 0-3000 ms time window, with one power image per condition being generated for each participant. These images were smoothed using a 12 mm Gaussian kernel and entered into a second-level random effects (1x3) ANOVA in SPM to investigate power differences across conditions. Small volume correction was performed using a bilateral hippocampus mask generated from the AAL atlas implemented in the WFU PickAtlas software (http://fmri.wfubmc.edu/software/pickatlas). Identification of activation peaks in other regions was performed using the AAL atlas (Tzourio-Mazoyer et al., 2002). This analysis was repeated in the alpha (9-12 Hz) and gamma (31-85 Hz) bands to investigate task-based modulation of these frequencies.

We hypothesised that mental imagery would be associated with anterior rather than posterior hippocampal activation (Dalton et al., 2018; Hassabis et al., 2007b; Zeidman et al., 2015; Zeidman and Maguire, 2016). To test this hypothesis more thoroughly, we divided a left hippocampal mask into anterior, middle and posterior segments of equal length. We extracted the mean percentage difference in theta power between our imagery conditions and the counting baseline for each segment and participant. For each subject, we then performed a linear regression with hippocampal segment as the predictor variable and the difference in theta power from baseline as the dependent variable.

Coherence

Coherent activity between sources was measured using the Dynamic Imaging of Coherent Sources (DICS) approach (Gross et al., 2001). In this case, a beamformer reference signal estimate is first performed for a reference location, in this case a defined source in the anterior hippocampus. This analysis was performed separately in the 4-8 Hz and 9-12 Hz bands within the 3000 ms task time window. Then scanning the brain on a 3 mm grid, a signal estimate was made at each location and

283 the coherence between this signal and the reference (in either the 4-8 Hz or 9-12 Hz bands)
284 computed. These values were output as an image for each condition representing a brain-wide map
285 of coherent activity with the reference source. These images were smoothed using a 12 mm
286 Gaussian kernel, and contrasts between conditions at the group level were performed using a
287 second-level random effects paired t-test in SPM.
288
289 For subsequent analyses, time series of theta activity during the 3000 ms imagery task period were
290 extracted from two 10 mm radius spheres encompassing the hippocampal reference source and the
291 group coherence peak in the vmPFC using the LCMV beamforming algorithm. To compare theta
292 coherence between scene trials which were subsequently remembered in the post-scan recognition
293 memory test, with scene trials that were forgotten, we performed a coherence analysis on the
294 extracted time series of remembered and forgotten trials, via the *mscohere* function in the Matlab
295 signal toolbox, using Welch's averaged modified periodogram method. The imagination period was
296 divided into three one second epochs with no overlap, and coherence was calculated over the
297 frequency range of 4-8 Hz. One participant successfully recognised all 75 scene stimuli and was
298 therefore excluded from this analysis. The same analysis was performed on scene trials which were
299 imagined in high versus low detail. Given strong *a priori* hypotheses from previous research that
300 theta coherence would be positively associated with subsequent memory performance (Backus et
301 al., 2016), and highly detailed visual imagery (Fuentemilla et al., 2014), we performed a one-sided
302 paired t-test in both cases.
303
304 ***Effective connectivity***
305 To determine effective connectivity, we utilised DCM for Cross Spectral Densities (Moran et al.,
306 2009), which analyses the magnitude of cross spectra between regions. The DCM approach involves
307 creating a model specifying the direction of inter-regional information flow and fitting this model to
308 the actual neural data. Multiple possible models can be generated and compared in the same

309 manner to ascertain the best explanation for the experimental observations. DCM for MEG uses a
310 biophysical neural-mass model which attempts to summarise the activity of millions of neurons
311 within a region. This model accommodates different neuronal types and their intrinsic connectivity,
312 treating the measurable output of these cell populations as a convolution of their input. If a region
313 is being causally influenced by another, this activity should change in a predictable manner based on
314 the nature of afferent input from the source. These inputs are characterised as forward, or "bottom
315 up", if they project to the middle layers of the cortex, backward, or "top down" if they target deep
316 and superficial layers, or lateral if they innervate all layers (Felleman and Van Essen, 1991). One can
317 therefore test biologically plausible models based on known structural connections between two
318 regions, that differ in terms of which connections are functionally modulated by the experimental
319 task.
320
321 The DCM estimation process attempts to fit these different models to the observed data as closely
322 as possible by tuning their parameters. The evidence for any one model represents a balance
323 between how accurate and parsimonious it is in explaining the data, as models with too many
324 parameters are penalised. In this study, we used a convolution-based local field potential (LFP)
325 neuronal model, as this is the simplest and most efficient approach when addressing hypotheses
326 regarding differences in effective extrinsic connectivity (Moran et al., 2013). To assess which model
327 best explains the observed data on a group level, random effects Bayesian model comparison
328 (Stephan et al., 2009) is performed, which compares the evidence for each model across all
329 participants, and generates the probability of it being the winning model. To assess the quality and
330 consistency of model fit, we generated the log Bayes factor for each participant separately by
331 computing the difference between the log evidence of the two models.
332
333 ***Event-related spectral perturbations***
334 To further exploit the fine temporal resolution of MEG, we performed an additional analysis on the

time-course of theta power changes across the scene imagination period. Using the same source-extracted time-series of activity in the vmPFC and anterior hippocampus, we applied a Morlet wavelet-based time frequency analysis with seven wavelet cycles across the 4-8 Hz frequency range. The time-period of interest extended from 500 ms prior to cue offset until the end of the 3000 ms imagination period (padded with real data). This was performed separately on each trial and subsequently averaged. The averaged time-frequency decomposition of the 0-3000 ms task period was then converted into log power, baseline corrected and transformed into dB values by rescaling to the 500 ms pre-task period. We then collapsed across frequency to produce a single time-series of event-related theta power changes in both regions. This time series was then smoothed using a 250 ms Gaussian kernel to attenuate variability in the temporal response across participants. The smoothed time series were entered into a random effects second level SPM analysis, generating a group F value at each time-point, with correction for multiple comparisons set at FWE $p < 0.05$.

Results

Behavioural

In-scanner task performance

Participants' in-scanner self-rated performance was high (Table 2), with a minimal proportion of trials rated as unsuccessful. Of the trials eligible for subsequent analysis, there was a similar proportion of scene imagery, object imagery and counting trials ($F_{(1.22,25.64)} = 2.25$, $p = 0.142$). Scene and object stimuli appeared to successfully evoke the intended mental imagery, as a comparably low percentage of trials were reclassified in the two conditions ($t_{(21)} = -1.67$, $p = 0.110$). The majority of scenes and objects were imagined in high detail with both conditions matched on this rating ($t_{(21)} = -1.33$, $p = 0.199$). Furthermore, for most counting trials, concentration was rated as high (>3/5), indicating participants successfully maintained their attention during this baseline condition.

361 ***Post-scan recognition memory test***

362 Participants were able to correctly recognise most of the scene and object stimuli that they
363 previously imagined in the scanner, performing significantly above chance level in both conditions
364 (Table 3). They remembered a greater proportion of objects than scenes ($t_{(21)} = -2.10$, $p = 0.048$). In
365 addition, d' scores indicated that participants were significantly less accurate in distinguishing
366 between new and old scene compared to object words ($t_{(21)} = -4.19$, $p < 0.001$). Superior recognition
367 memory for objects corroborates the findings of Clark et al. (2018), and implies that a greater power
368 change or heightened connectivity during scene imagination relative to object imagination could not
369 be attributable to better encoding of scenes. Of note, c values for both scene and object words
370 indicated participants were conservative in their endorsement of recognised stimuli, in other words,
371 they tended to only respond as such when they were confident in their response. Responses were
372 more conservative for object than scene stimuli ($t_{(21)} = -3.61$, $p = 0.002$).

373

374 **MEG**

375 ***Source space power changes during mental imagery***

376 We first determined which brain regions were active during imagination in general, that is, scene
377 and object imagination tasks combined compared to the low-level counting condition. Due to the
378 obvious disparity in task demands between the imagery and baseline conditions, we used a
379 conservative whole brain family-wise error corrected threshold of $p < 0.001$. A widespread change in
380 theta power was observed during mental imagery when compared to the baseline task (Figure 2A).
381 This was evident throughout the left anterior temporal lobe, with an activation peak at the whole-
382 brain level in the inferior frontal gyrus (x = -38; y = 24, z = -4; Z-score = 6.23). Our primary *a priori*
383 region of interest was the anterior hippocampus, where a significant change from baseline was also
384 observed. A subsequent t-contrast revealed the observed changes represented an attenuation of
385 theta power during imagination rather than an increase from baseline. Nonetheless, we regarded
386 these power changes as an indication of task-related neural activity, and for subsequent connectivity

387 analyses we did not exclude the possibility of inter-regional coherence in the presence of lower
388 power. Subsequent small volume correction revealed an overall peak (-32, -4, -28; Z = 5.82) and sub-
389 peak (-32, -6, -22; Z = 5.61) in the left anterior hippocampus.
390
391 ***Gradient of theta power changes along the hippocampal longitudinal axis***
392 Having observed changes in theta power in the anterior hippocampus at the group level, we
393 investigated the consistency of this spatial selectivity across participants. We assessed each
394 participant's imagery-induced power change as a function of hippocampal segment (anterior, middle
395 or posterior). Across the group, the regression was significant ($F_{(1,64)} = 5.787$, $p = 0.019$), with
396 hippocampal segment explaining 8.3% of the variance in power difference between conditions.
397 Fifteen of the 22 participants displayed a linear gradient of activation along the anterior to posterior
398 hippocampal axis (Figure 3).
399
400 As the overall anterior hippocampal theta peak closely bordered the perirhinal cortex and fusiform
401 gyrus, the more dorsal and posterior sub-peak (Figure 2A, black circle) was selected for connectivity
402 analyses in order to be confident that source-localised activity originated from the hippocampus.
403 This is because despite the fine spatial resolution of MEG beamforming, the volumetric full-width
404 half-maximum (FWHM) of activation is on the order of at least a few millimetres (Barnes et al.,
405 2004). Of note, no difference in theta power was observed at the whole brain level between scene
406 and object imagination, even using an exploratory uncorrected threshold of $p < 0.005$ (cluster size >
407 5), or within the hippocampus in an ROI analysis ($p < 0.05$ uncorrected). In summary, scene and
408 object imagery appeared to engage a common network of brain regions to a similar degree,
409 including the anterior hippocampus. Therefore, any observed differences in connectivity between
410 the two imagery conditions could not be explained by differences in power. Consequently, in the
411 subsequent coherence analysis, we were able to directly explore the changes in network
412 connectivity due to imagining scenes rather than single objects.

To investigate if there was a change in other frequency bands during our imagination tasks, we performed identical source localisation analyses across alpha (9-12 Hz) and gamma (31-85 Hz) frequencies. Significant changes in alpha power were observed in the medial temporal lobe, and small volume correction identified a single peak of activity in the anterior hippocampus (-24, -6, -26; Z = 5.53; Figure 2B). No differences in gamma power were observed between the imagery and baseline conditions at a FWE-corrected threshold of $p < 0.05$. The spatial proximity of alpha and theta power decreases in the anterior hippocampus allowed us to ascertain the specificity of the theta band rhythm in subsequent analyses of coherence, by using both peaks as a connectivity seed.

Hippocampal connectivity during scene imagery

Having established the peak locations of power changes in the anterior hippocampus during mental imagery, we then sought to investigate whether the imagination of scenes was associated with greater connectivity with any other regions of the brain when compared to object imagination. We found higher theta coherence in the left fusiform gyrus (Figure 4A; peak voxel: -32, -18, -32; Z = 3.58, $p < 0.001$ uncorrected) and parahippocampal cortex (peak voxel: -32, -38, -14; Z = 3.47, $p < 0.001$ uncorrected) during scene imagery. Given that we had a specific *a priori* hypothesis regarding connectivity between the hippocampus and vmPFC for scene imagery, we applied an uncorrected threshold of $p < 0.005$, and discovered a bilateral cluster of voxels coherent with the hippocampal source, at the most ventral extent of the vmPFC (Figure 4B; peak voxel: 18, 34, -16; Z = 2.87), with a sub-peak in the left vmPFC (-2, 46, - 28; Z = 2.86). This left-sided vmPFC peak was used for subsequent anatomically-informed analyses of effective connectivity as the hippocampus and vmPFC are connected ipsilaterally. Of note, the reverse contrast (greater connectivity for objects than scenes) did not reveal any significant results throughout the whole brain at a significance level of $p < 0.005$. Furthermore, at this threshold we did not observe higher coherence in the scene condition between the anterior hippocampus and other regions previously implicated in scene construction

439 such as the precuneus, retrosplenial cortex, calcarine sulcus or occipital gyrus.

440

441 To determine whether this increased coherence for scenes over objects was specific to the theta
442 oscillation, we also used the location of peak alpha power change in the anterior hippocampus as a
443 seed for brain-wide coherence in the alpha band. We did not find any region coherent with the
444 hippocampus at a threshold of $p < 0.001$ (uncorrected), nor was coherent activity with the vmPFC
445 observed at a threshold of $p < 0.005$ (uncorrected).

446

447 Our primary hypothesis was that scene construction and episodic memory are subserved by similar
448 interactions between the hippocampus and the vmPFC. To make this direct comparison, we
449 compared the theta coherence of imagined scenes which were subsequently remembered in the
450 post-scan recognition test, with those that were forgotten. In support of our hypothesis, coherence
451 between the two regions was higher for imagined scenes which were also successfully memorised
452 ($t_{(20)} = 2.25$, $p = 0.018$; Figure 4C), despite the absence of any explicit instruction to do so. One
453 potential interpretation of higher coherence in the scene construction condition is that it is a more
454 effortful task than object construction. If this were the case, scenes imagined in low detail, which
455 arguably serves as a proxy for difficulty, would show greater connectivity between the hippocampus
456 and vmPFC. However, the opposite trend was observed, where coherence between the two regions
457 was greater for high detail when compared to low detail scenes, a difference which approached
458 significance ($t_{(21)} = 1.64$, $p = 0.058$; Figure 4D).

459

460 ***Effective connectivity during scene imagery***

461 Having established higher theta coherence between hippocampus and vmPFC during scene
462 imagination, we then investigated the directionality of information flow between the two regions.
463 Using DCM for Cross Spectral Densities, we first specified a biologically plausible model of
464 hippocampal-vmPFC connectivity. As the anterior hippocampus projects directly to the middle

465 layers of the ventral extent of the ipsilateral vmPFC (where we observed high theta coherence) via
466 the fornix (Aggleton et al., 2015), we designated this connection as forward. Because return
467 projections are indirectly channeled through the entorhinal cortex (EC), vmPFC influence over the
468 hippocampus is best characterised by the pattern of laminar innervation in EC. vmPFC efferents
469 terminate in all layers of EC (Rempel-Clower and Barbas, 2000), and consequently we designated the
470 return connection as lateral (Felleman and Van Essen, 1991). Additional thalamic relays exist
471 between the two structures (Varela et al., 2014; Xiao et al., 2009) but are not considered here as the
472 hierarchical nature of this connection type is unclear (Bastos et al., 2012).
473
474 Of key interest was the predominant direction of information flow between hippocampus and
475 vmPFC during scene imagination. Therfore we proposed two anatomically informed models. In
476 model 1, hippocampal activity drove the vmPFC via its forward connection. In model 2, lateral
477 projections from the vmPFC modulated activity of the hippocampus (Figure 5A). The specified time
478 period was the 3000 ms imagination task, and analysis of cross spectral density was constrained to
479 the theta (4-8Hz) frequency band to retain consistency with previous power and coherence analyses.
480 We applied both models to the observed data, and subsequently performed Bayesian model
481 comparison to determine which model was most likely to explain the relationship between the two
482 regions. The model most likely to be the winning model across all subjects, with a probability of
483 97.66%, was the vmPFC exerting a causal influence over the anterior hippocampus during the
484 imagination of novel scenes (Figure 5B).
485
486 To quantify the consistency of model fit, we calculated the log Bayes factor for each model and
487 participant separately (Figure 5C). According to the classification of Kass and Raftery (1995), a Bayes
488 factor of 3 to 20 (log equivalent 1.1 to 3) constitutes positive evidence in favour of a model, with
489 higher values indicating strong evidence. Eleven of the 22 participants in this study displayed
490 positive or strong evidence for vmPFC driving hippocampus (Figure 5C, blue bars). In contrast,

evidence for hippocampus driving the vmPFC was only present in two participants (green bars). In the remainder of the sample, there was no conclusive evidence for either model (grey bars).

Event-related spectral perturbations

In a complementary analysis to fully leverage the temporal precision of MEG, we compared the timing of neural responses in the vmPFC and hippocampus during the scene construction task. We charted the change in theta power over three seconds of scene imagery, relative to 500 ms preceding the offset of the cue (Figure 6). Overall peak activations (at a FWE-corrected threshold of $p < 0.05$) of the hippocampus (806 ms, Z = 3.72, bold yellow line) and vmPFC (899 ms, Z = 3.77, bold red line) were temporally proximal. However a much earlier sub-peak was observed in the vmPFC 310 milliseconds (Z = 3.19) following the offset of the cue. An additional peak of activity was observed in the vmPFC at a later point in the trial (1752 ms, Z = 3.68). The rapid initial engagement of the vmPFC in contrast to the slower kinetics of hippocampal activation provides additional evidence that the vmPFC may drive hippocampal activity to facilitate the construction of scene imagery.

Discussion

This study investigated whether the imagination of novel scenes is supported by a hippocampal-vmPFC dialogue. Mental imagery, whether of spatially-coherent scenes or isolated objects, resulted in comparable theta power decreases in the left anterior hippocampus. However, theta coherence between anterior hippocampus and vmPFC was significantly higher for scene compared to object imagination, and was of a greater magnitude for scenes that were subsequently remembered, or imagined in high detail. The observed coherence was also specific to the theta band. In addition, DCM of this interaction revealed the vmPFC drove hippocampal activity during the scene construction process, and an analysis of event-related spectral perturbations showed that the activity of vmPFC preceded that of hippocampus.

These findings corroborate fMRI studies demonstrating that the anterior hippocampus contributes to the mental construction of novel scene imagery (Hassabis et al., 2007b; Zeidman et al., 2015; Zeidman and Maguire, 2016, Dalton et al., 2018). An interesting feature of our data, which contradicts some previous reports of theta increases during learning and episodic memory tasks, is the attenuation of this frequency during imagination. However, evidence has accumulated from electroencephalography (EEG; Fellner et al., 2016) and MEG (Guderian et al., 2009) demonstrating a strong decrease in medial temporal lobe theta during episodic memory encoding. These findings have been validated using direct intracranial recordings in humans, with brain-wide decreases in theta power predicting subsequent recall (Burke et al., 2013; Greenberg et al., 2015), and specifically in the hippocampus (Sederberg et al., 2007; Lega et al., 2012; Matsumoto et al., 2013; Lega et al., 2017). A decrease in 8Hz power has also been reported during episodic memory retrieval (Michelmann et al., 2016). Furthermore, decreases in low frequency power appear to be negatively correlated with the fMRI BOLD response (Fellner et al., 2016; Scheeringa et al., 2011), and, therefore, our findings may be consistent with observed BOLD increases in previous fMRI studies.

The functional significance of the observed theta power decrease is not yet clear. However, in rodents, reduced hippocampal theta power is observed upon introduction to a novel or unexpected environment (Jeewajee et al., 2008). Our task involved the rapid mental construction of novel scenes (and so environments) in response to unpredictable stimuli, and the underlying oscillatory dynamics may, therefore, be similar. Importantly, a lower amplitude signal can still contain rich information about the underlying mental representations during episodic memory retrieval (Michelmann et al., 2016).

In the current study, theta power in the hippocampus did not differentiate between scene and object imagination. This accords with recent fMRI findings showing that object stimuli engage the

543 hippocampus (Clark et al., 2018; Dalton et al., 2018), and that different task and stimulus-specific
544 circuits may exist within the hippocampus, which receive distinct cortical afferents. Concordantly,
545 Fuentemilla et al. (2014) demonstrated that while hippocampal theta power was similar during the
546 retrieval of semantic and autobiographical memories, connectivity with the vmPFC was higher
547 during the latter hippocampal-dependent task. Likewise, we observed increased theta coherence
548 between the anterior hippocampus and vmPFC during scene, more so than object, construction,
549 indicating a similar network dynamic may support episodic memory retrieval and scene imagination.
550 Providing further support for such a shared dynamic, we discovered that the magnitude of
551 coherence between these two regions during scene imagination predicted whether or not the
552 stimulus was subsequently remembered.
553
554 How might the vmPFC facilitate both processes? The vmPFC is a proposed target of systems-level
555 memory consolidation and long-term storage (Nieuwenhuis and Takashima, 2011), with evidence in
556 humans of the reactivation of specific remote autobiographical memory traces (Bonnici et al., 2012;
557 Barry et al., 2018). Yet participants in the current study were instructed to avoid recalling a specific
558 autobiographical memory during the imagination process. However, the vmPFC is also thought to
559 slowly extract regularities across past experiences to form superordinate representations, or
560 schemas (van Kesteren et al., 2013; Gilboa and Marlatte, 2017). These may serve as flexible
561 conceptual "templates" within which to rapidly and efficiently construct spatially coherent novel
562 scenes in concert with the hippocampus.
563
564 Patients with vmPFC damage have schema-related deficits (Ciaramelli et al. 2006; Gilboa et al, 2006;
565 Ghosh et al., 2014; Warren et al., 2014) and are impaired at constructing scene imagery (Bertossi et
566 al., 2016a; Bertossi et al., 2016b; Bertossi et al., 2017; De Luca et al., 2018). However, such patients
567 can generate imagery for individual scenes from autobiographical events in response to highly
568 specific cues (Kurczek et al., 2015). Consequently, and in keeping with its role in supporting schema,

569 it has been suggested that the vmPFC is necessary to select appropriate elements for a particular
570 scene, while the hippocampus is needed to construct the scene imagery (McCormick et al., 2018).
571 Our results are compatible with this interpretation, as coherence between the two regions was of a
572 greater magnitude for scenes which were imagined in high detail.
573
574 An ensuing question is how the two brain regions collaborate to produce these integrated
575 representations. One interpretation is that during imagination, the role of the vmPFC is to fuse
576 distributed knowledge into a novel representation (Benoit et al., 2014), with corresponding evidence
577 from fMRI that the hippocampus drives activity in the vmPFC when simulating the future (Campbell
578 et al., 2018). However, an alternate perspective, as alluded to above, holds that the vmPFC exerts
579 direct control over the hippocampus to select context-relevant representations (Eichenbaum, 2017;
580 McCormick et al., 2018). Our finding of vmPFC exerting a causal influence over the hippocampus
581 during scene imagination is more consistent with this latter view. We also regard MEG as a method
582 well-suited to characterising this relationship given that it is a direct and time-resolved measure of
583 neural activity.
584
585 What aspects of the lateral projection from vmPFC are influencing the hippocampus remains an
586 open question. The preferential termination of neurons in the middle layers of the entorhinal cortex
587 (Rempel-Clower and Barbas, 2000) indicates the presence of a driving and excitatory input (Bastos et
588 al., 2012) to the hippocampus. Conversely, the majority of residual connections project to inhibitory
589 neurons in the deepest layers (Joyce and Barbas, 2018), suggesting vmPFC also heavily constrains
590 hippocampal output. From a behavioural perspective, the inability of patients with vmPFC damage
591 to retrieve context-relevant information during scene construction tasks (Bertossi et al., 2016a) –
592 which involve cues that are relatively unconstrained (Hassabis et al., 2007a) – while being also
593 unable to suppress context-irrelevant information while confabulating (Turner et al., 2008), suggests
594 the vmPFC may control both hippocampal input and output during scene imagination. Our time-

resolved analysis of vmPFC activity during the construction of novel scenes identified additional periods of early and late engagement relative to hippocampal activation, adding credence to this view.

Our results also revealed that engaging in mental imagery in response to scene and object words relative to the counting baseline resulted in power decreases in the left inferior frontal gyrus. This activation peak was localised to Brodmann Area 47, a region implicated in the processing of verbal stimuli (Krieger-Redwood et al., 2015), in particular single words (Cutting et al., 2006). As this activation was common to scene and object words, it likely reflects the increased demands in semantic processing relative to the number stimuli in the baseline counting condition. This lexical processing is likely to be contemporaneous with mental imagery (Lewis and Poeppel, 2014), and it is therefore unlikely that word comprehension and imagination in the current experiment are temporally dissociable.

One additional finding which differentiated scene from object construction was increased theta coherence between the anterior hippocampus and the fusiform and parahippocampal cortices. Increased fusiform activity has also been observed in a separate fMRI study involving the scene word stimuli used in the current experiment (Clark et al., 2018). This region appears to represent diverse categories of objects, living beings and their interactions (Grill-Spector et al., 2006; Cukur et al., 2013), and scenes represent the coherent integration of these constituent elements. Observed coherence with the parahippocampal cortex during scene imagination is consistent with the parahippocampal cortex's proposed role in processing scenes (Epstein, 2008; Mullally and Maguire, 2011). This connectivity profile, therefore, suggests that the anterior hippocampus may be a convergence zone for appropriate object categories and their interaction within a defined space, permitting the generation of scene imagery (Dalton and Maguire, 2017).

621 In summary, our results characterise, for the first time, a core neural dynamic which underlies scene
622 construction, a process held by some to be fundamental to key cognitive functions including episodic
623 memory and future-thinking. Previous studies have demonstrated co-activation of (Hassabis et al.,
624 2007b), and a dependency on (Hassabis et al., 2007a; Bertossi et al., 2016a), the hippocampus and
625 vmPFC during scene construction. By leveraging the high temporal resolution of MEG, we have
626 extended these findings to demonstrate their functional connectivity during this process.
627 Furthermore, we have shown that the direction of information flow during scene imagination
628 mirrors that observed during episodic memory retrieval (Place et al., 2016), with vmPFC driving
629 hippocampal activity. We conclude that episodic memory and imagination share fundamental
630 neural dynamics, and the process of constructing vivid, spatially coherent, contextually appropriate
631 scene imagery is strongly modulated by the vmPFC.

632

633 **References**

634 Aggleton JP, Wright NF, Rosene DL, Saunders RC (2015) Complementary patterns of direct amygdala
635 and hippocampal projections to the macaque prefrontal cortex. Cereb Cortex 25:4351-4373.
636 Backus A, Schoffelen JM, Szebenyi S, Hanslmayr S., Doeller C F (2016) Hippocampal-prefrontal theta
637 oscillations support memory integration. Curr Biol 26:450-457.
638 Balota DA, Yap MJ, Hutchison KA, Cortese MJ, Kessler B, Loftis B, Neely JH, Nelson DL, Simpson GB,
639 Treiman R (2007) The english lexicon project. Behav Res Methods 39:445-459.
640 Barnes GR, Hillebrand A, Fawcett IP, Singh KD (2004). Realistic spatial sampling for MEG beamformer
641 images. Hum Brain Mapp 23:120-127.
642 Barry DN, Chadwick MJ, Maguire EA (2018) Nonmonotonic recruitment of ventromedial prefrontal
643 cortex during remote memory recall. PLoS Biol 16:e2005479.
644 Bastos AM, Usrey WM, Adams RA, Mangun GR, Fries P, Friston KJ (2012) Canonical microcircuits for
645 predictive coding. Neuron 76:695-711.
646 Benoit RG, Szpunar KK, Schacter DL (2014) Ventromedial prefrontal cortex supports affective future
647 simulation by integrating distributed knowledge. Proc Natl Acad Sci U S A 111:16550-16555.
648 Bertossi E, Aleo F, Braghittoni D, Ciaramelli E (2016a) Stuck in the here and now: Construction of
649 fictitious and future experiences following ventromedial prefrontal damage.
650 Neuropsychologia 81:107-116.
651 Bertossi E, Tesini C, Cappelli A, Ciaramelli E (2016b) Ventromedial prefrontal damage causes a
652 pervasive impairment of episodic memory and future thinking. Neuropsychologia 90:12-24.
653 Bertossi E, Candela V, De Luca F, Ciaramelli E (2017). Episodic future thinking following vmPFC
654 damage: Impaired event construction, maintenance, or narration? Neuropsychology 31:337-
655 348.
656 Bonnici HM, Chadwick MJ, Lutti A, Hassabis D, Weiskopf N, Maguire EA (2012) Detecting
657 representations of recent and remote autobiographical memories in vmPFC and
658 hippocampus. J Neurosci 32:16982-16991.

Brysbaert M, Warriner AB, Kuperman V (2014) Concreteness ratings for 40 thousand generally known English word lemmas. Behav Res Methods 46:904-911.
Buckner RL (2010) The role of the hippocampus in prediction and imagination. Annu Rev Psychol 27-48:C21-28.
Burke JF, Zaghloul KA, Jacobs J, Williams RB, Sperling MR, Sharan AD, Kahana MJ (2013) Synchronous and asynchronous theta and gamma activity during episodic memory formation. J Neurosci 33:292-304.
Campbell KL, Madore KP, Benoit RG, Thakral PP, Schacter DL (2018) Increased hippocampus to ventromedial prefrontal connectivity during the construction of episodic future events. Hippocampus 28:76-80.
Ciaramelli E, Ghetti S, Frattarelli M, Ladavas E (2006) When true memory availability promotes false memory: evidence from confabulating patients. Neuropsychologia 44:1866-1877.
Clark IA, Kim M, Maguire EA (2018) Verbal paired associates and the hippocampus: the role of scenes. J Cogn Neurosci 30:1821-1845.
Cukur T, Huth AG, Nishimoto S, Gallant JL (2013) Functional subdomains within human FFA. J Neurosci 33:16748-16766.
Cutting LE, Clements AM, Courtney S, Rimrodt SL, Schafer JG, Bisesi J, Pekar JJ, Pugh KR (2006) Differential components of sentence comprehension: beyond single word reading and memory. Neuroimage 29:429-438.
Dalton MA, Maguire EA (2017) The pre/parasubiculum: a hippocampal hub for scene-based cognition? Curr Opin Behav Sci 17:34-40.
Dalton MA, Zeidman P, McCormick C, Maguire, EA (2018) Differentiable processing of objects, associations and scenes within the hippocampus. J Neurosci 38:8146-8159.
de Borst, AW, Sack AT, Jansma BM, Esposito F, de Martino F, Valente G, Roebroeck A, di Salle F, Goebel R, Formisano, E (2012) Integration of “what” and “where” in frontal cortex during visual imagery of scenes. Neuroimage 60:47-58.
De Luca F, McCormick C, Mullally SL, Intraub H, Maguire EA, Ciaramelli E (2018) Boundary extension is attenuated in patients with ventromedial prefrontal cortex damage. Cortex 108:1-12.
Eichenbaum H (2017) Prefrontal-hippocampal interactions in episodic memory. Nature Rev Neurosci 18:547-558.
Eichenbaum H, Fortin NJ (2009) The neurobiology of memory based predictions. Philos Trans R Soc B 364:1183-1191.
Epstein RA (2008) Parahippocampal and retrosplenial contributions to human spatial navigation. Trends Cogn Sci 12:388-396.
Felleman DJ, Van Essen DC (1991) Distributed hierarchical processing in the primate cerebral cortex. Cereb Cortex 1:1-47.
Fellner MC, Volberg G, Wimber M, Goldhacker M, Greenlee MW, Hanslmayr S (2016) Spatial mnemonic encoding: Theta power decreases and medial temporal lobe BOLD increases co-occur during the usage of the method of loci. eNeuro 3:e0184-16.2016.
Fries P (2005). A mechanism for cognitive dynamics: neuronal communication through neuronal coherence. Trends Cogn Sci 9:474-480.
Friston KJ, Harrison L, Penny W (2003) Dynamic causal modelling. Neuroimage 19:1273-1302.
Fuentemilla L, Barnes GR, Duzel E, Levine B (2014) Theta oscillations orchestrate medial temporal lobe and neocortex in remembering autobiographical memories. Neuroimage 85:730-737.
Garrido MI, Barnes GR, Kumaran D, Maguire EA, Dolan RJ (2015) Ventromedial prefrontal cortex drives hippocampal theta oscillations induced by mismatch computations. Neuroimage, 120:362-370.
Ghosh VE, Moscovitch M, Melo Colella B, Gilboa A (2014) Schema representation in patients with ventromedial PFC lesions. J Neurosci 34:12057-12070.
Gilboa A, Alain C, Stuss DT, Melo B, Miller S, Moscovitch M (2006) Mechanisms of spontaneous confabulations: a strategic retrieval account. Brain 129:1399-1414.

Gilboa A, Marlatte H (2017) Neurobiology of schemas and schema-mediated memory. Trends Cogn Sci 21:618-631.
Greenberg JA, Burke JF, Haque R, Kahana MJ, Zaghloul KA (2015) Decreases in theta and increases in high frequency activity underlie associative memory encoding. Neuroimage 114:257-263.
Grill-Spector K, Sayres R, Ress D (2006) High-resolution imaging reveals highly selective nonface clusters in the fusiform face area. Nat Neurosci 9:1177.
Gross J, Kujala J, Hämäläinen L, Timmermann L, Schnitzler A, Salmelin R (2001) Dynamic imaging of coherent sources: studying neural interactions in the human brain. Proc Natl Acad Sci U S A 98: 694-699.
Guderian S, Schott BH, Richardson-Klavehn A, Duzel E (2009) Medial temporal theta state before an event predicts episodic encoding success in humans. Proc Natl Acad Sci U S A 106:5365-5370.
Guitart-Masip M, Barnes GR, Horner A, Bauer M, Dolan RJ, Duzel E (2013) Synchronization of medial temporal lobe and prefrontal rhythms in human decision making. J Neurosci 33:442-451.
Hassabis D, Maguire EA (2007) Deconstructing episodic memory with construction. Trends Cogn Sci 11: 299-306.
Hassabis D, Kumaran D, Vann SD, Maguire EA (2007a) Patients with hippocampal amnesia cannot imagine new experiences. Proc Natl Acad Sci U S A 104:1726-1731.
Hassabis D, Kumaran D, Maguire, EA (2007b) Using imagination to understand the neural basis of episodic memory. J Neurosci 27:14365-14374.
Jeewajee A, Lever C, Burton S, O'Keefe J, Burgess N (2008) Environmental novelty is signaled by reduction of the hippocampal theta frequency. Hippocampus 18:340-348.
Joyce MKP, Barbas H (2018). Cortical connections position primate area 25 as a keystone for interoception, emotion, and memory. J Neurosci 38:1677-1698.
Kaplan R, Bush D, Bonnefond M, Bandettini PA, Barnes GR, Doeller CF, Burgess N (2014) Medial prefrontal theta phase coupling during spatial memory retrieval. Hippocampus 24:656-665.
Krieger-Redwood K, Teige C, Davey J, Hymers M, Jefferies E (2015) Conceptual control across modalities: graded specialisation for pictures and words in inferior frontal and posterior temporal cortex. Neuropsychologia 76:92-107.
Kuperman V, Stadthagen-Gonzalez H, Brysbaert M (2012) Age-of-acquisition ratings for 30,000 English words. Behav Res Methods 44:978-990.
Kass RE, Raftery AE (1995) Bayes factors. J Am Stat Assoc 90:773-795.
Kwan D, Carson N, Addis DR, Rosenbaum RS (2010) Deficits in past remembering extend to future imagining in a case of developmental amnesia. Neuropsychologia 48:3179-3186.
Kurczek J, Wechsler E, Ahuja S, Jensen U, Cohen NJ, Tranel D, Duff M (2015) Differential contributions of hippocampus and medial prefrontal cortex to self-projection and self-referential processing. Neuropsychologia 73:116-126.
Lega BC, Germi J, Rugg M (2017) Modulation of oscillatory power and connectivity in the human posterior cingulate cortex supports the encoding and retrieval of episodic memories. J Cogn Neurosci 29:1415-1432.
Lega BC, Jacobs J, Kahana M (2012) Human hippocampal theta oscillations and the formation of episodic memories. Hippocampus 22:748-761.
Lesting J, Daldrup T, Narayanan V, Himpe C, Seidenbecher T, Pape HC (2013) Directional theta coherence in prefrontal cortical to amygdalo-hippocampal pathways signals fear extinction. PLoS One 8:e77707.
Lewis G, Poeppel D (2014) The role of visual representations during the lexical access of spoken words. Brain Lang 134:1-10.
Maguire EA, Mullally SL (2013) The hippocampus: a manifesto for change. J Exp Psychol Gen 142:1180-1189.

Matsumoto JY, Stead M, Kucewicz MT, Matsumoto AJ, Peters PA, Brinkmann BH, Marsh WR, Meyer FB, Worrell GA (2013) Network oscillations modulate interictal epileptiform spike rate during human memory. Brain 136:2444-2456.

McCormick C, Ciaramelli E, De Luca F, Maguire EA (2018) Comparing and contrasting the cognitive effects of hippocampal and ventromedial prefrontal cortex damage: A review of human lesion studies. Neuroscience 374:295–318.

Michelmann S, Bowman H, Hanslmayr S (2016) The temporal signature of memories: Identification of a general mechanism for dynamic memory replay in humans. PLoS Biol 14:e1002528.

Moran R, Pinotsis DA, Friston K (2013) Neural masses and fields in dynamic causal modeling. Front Comput Neurosci 7:57.

Moran RJ, Stephan KE, Seidenbecher T, Pape HC, Dolan RJ, Friston KJ (2009) Dynamic causal models of steady-state responses. Neuroimage 44:796-811.

Mullally SL, Maguire EA (2011) A new role for the parahippocampal cortex in representing space. J Neurosci 31:7441-7449.

Nieuwenhuis IL, Takashima A (2011) The role of the ventromedial prefrontal cortex in memory consolidation Behav Brain Res 218:325-334.

Nolte G (2003) The magnetic lead field theorem in the quasi-static approximation and its use for magnetoencephalography forward calculation in realistic volume conductors. Phys Med Biol 48:3637-3652.

Place R, Farovik A, Brockmann M, Eichenbaum H (2016) Bidirectional prefrontal-hippocampal interactions support context-guided memory. Nat Neurosci 19:992-994.

Rempel-Clower NL, Barbas H (2000) The laminar pattern of connections between prefrontal and anterior temporal cortices in the rhesus monkey is related to cortical structure and function. Cereb Cortex 10:851-865.

Schacter DL, Addis DR (2007) The cognitive neuroscience of constructive memory: remembering the past and imagining the future. Philos Trans R Soc B 362:773-786.

Scheeringa R, Fries P, Petersson KM, Oostenveld R, Grothe I, Norris DG, Hagoort P, Bastiaansen MCM (2011) Neuronal dynamics underlying high- and low-frequency EEG oscillations contribute independently to the human BOLD signal. Neuron 69:572-583.

Scoville WB, Milner B (1957) Loss of recent memory after bilateral hippocampal lesions. J Neurol Neurosurg Psychiatry 20:11-21.

Sederberg PB, Schulze-Bonhage A, Madsen JR, Bromfield, EB, McCarthy DC, Brandt A, Tully MS, Kahana MJ (2007) Hippocampal and neocortical gamma oscillations predict memory formation in humans. Cereb Cortex 17:1190-1196.

Stephan KE, Penny WD, Daunizeau J, Moran RJ, Friston KJ (2009) Bayesian model selection for group studies. Neuroimage 46:1004-1017.

Turner MS, Cipolotti L, Yousry TA, Shallice T (2008) Confabulation: damage to a specific inferior medial prefrontal system. Cortex 44:637-648.

Tzourio-Mazoyer N, Landeau B, Papathanassiou D, Crivello F, Etard O, Delcroix, N, Mazoyer B, Joliot M (2002) Automated anatomical labeling of activations in SPM using a macroscopic anatomical parcellation of the MNI MRI single-subject brain. Neuroimage 15:273-289.

van Heuven WJB, Mandera P, Keuleers E, Brysbaert M (2014) Subtlex-UK: a new and improved word frequency database for British English. Q J Exp Psychol 67:1176-1190.

van Kesteren MT, Beul SF, Takashima A, Henson RN, Ruiter DJ, Fernandez G (2013) Differential roles for medial prefrontal and medial temporal cortices in schema-dependent encoding: from congruent to incongruent. Neuropsychologia 51:2352-2359.

Varela C, Kumar S, Yang JY, Wilson MA (2014) Anatomical substrates for direct interactions between hippocampus, medial prefrontal cortex, and the thalamic nucleus reuniens. Brain Struct Funct 219:911-929.

Vigliocco G, Kousta ST, Della Rosa PA, Vinson DP, Tettamanti M, Devlin JT, Cappa SF (2014) The neural representation of abstract words: the role of emotion. Cereb Cortex 24:1767-1777.

Warren DE, Jones SH, Duff MC, Tranel D (2014) False recall is reduced by damage to the ventromedial prefrontal cortex: implications for understanding the neural correlates of schematic memory. J Neurosci 34:7677-7682.

Warriner AB, Kuperman V, Brysbaert M (2013) Norms of valence, arousal, and dominance for 13,915 English lemmas. Behav Res Methods 45:1191-1207.

Vincent JL, Snyder AZ, Fox MD, Shannon BJ, Andrews JR, Raichle ME, Buckner RL (2006) Coherent spontaneous activity identifies a hippocampal-parietal memory network. J Neurophysiol 96:3517-3531.

Xiao D, Zikopoulos B, Barbas H (2009) Laminar and modular organization of prefrontal projections to multiple thalamic nuclei. Neuroscience 161:1067-1081.

Zeidman P, Maguire EA (2016) Anterior hippocampus: the anatomy of perception, imagination and episodic memory. Nature Rev Neurosci 17:173-182.

Zeidman P, Mullally SL, Maguire EA (2015) Constructing, perceiving, and maintaining scenes: hippocampal activity and connectivity. Cereb Cortex 25:3836-3855.

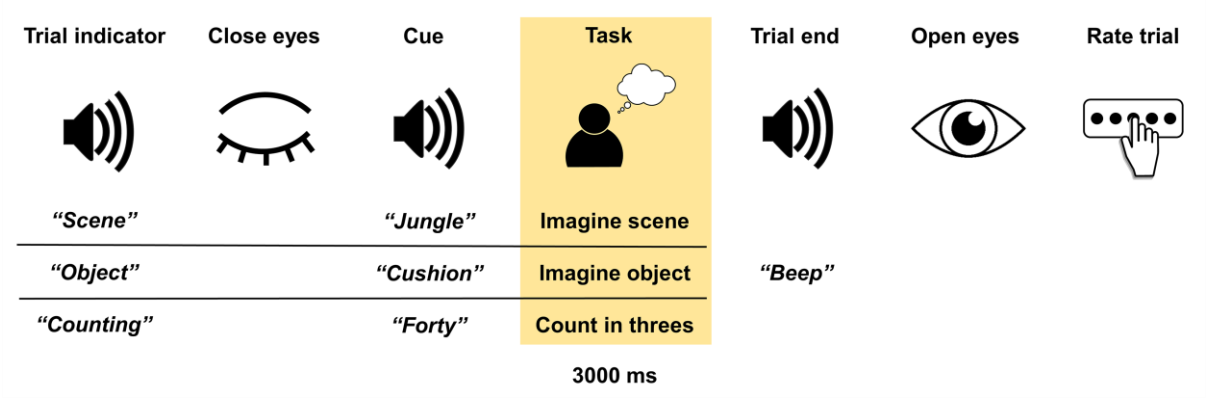

Figure 1. Trial structure. The task period selected for analysis is highlighted.

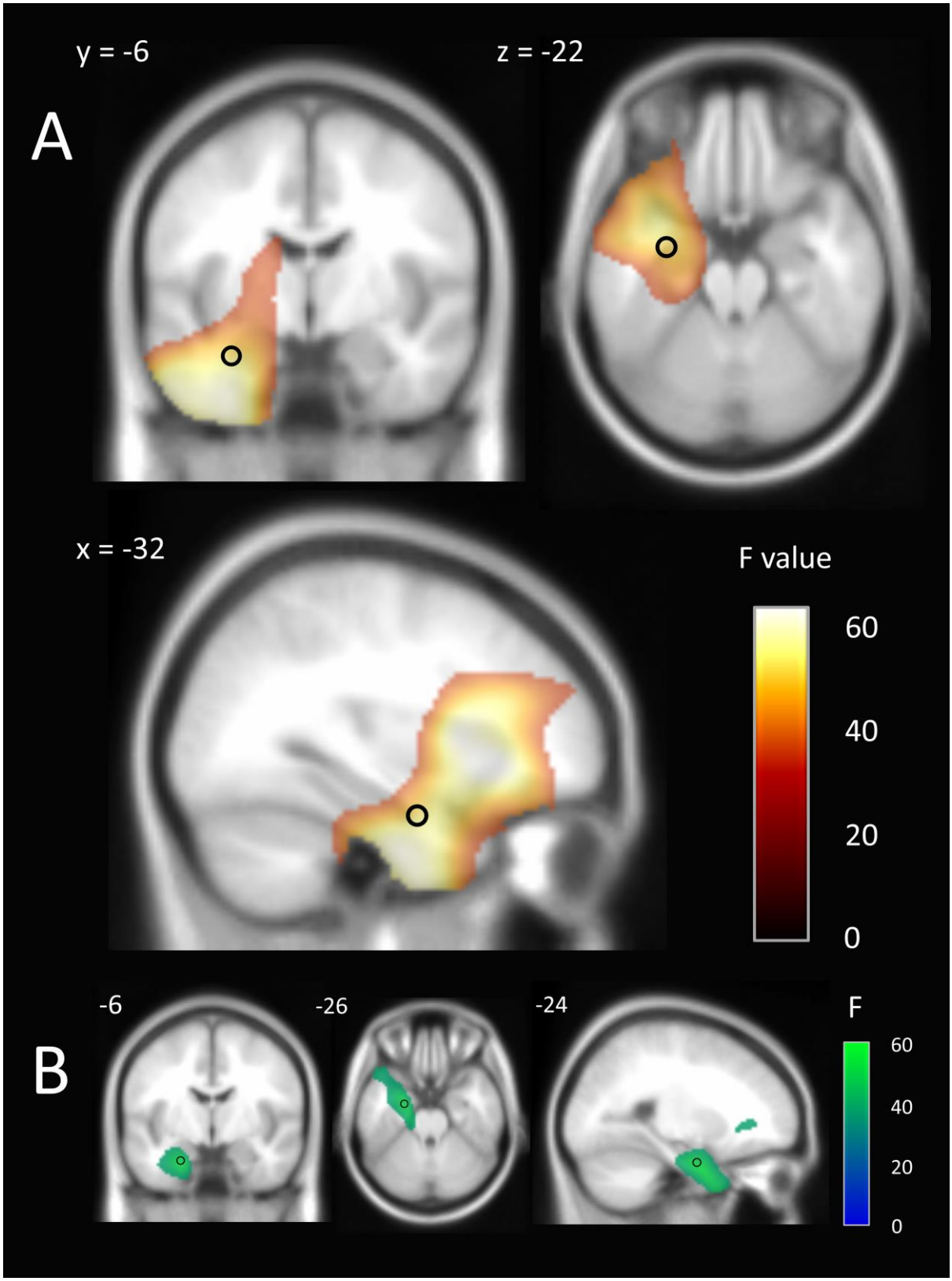

Figure 2. MEG source reconstruction of theta (4-8 Hz) and alpha (9-12 Hz) power changes during mental imagery (scenes and objects) compared to the baseline condition. The black circles represent the peak location of theta (A) and alpha (B) power changes in anterior hippocampus used for subsequent connectivity analyses. Images are FWE thresholded at $p < 0.001$ and superimposed on the Montreal Neurological Institute (MNI) 152 T1 image.

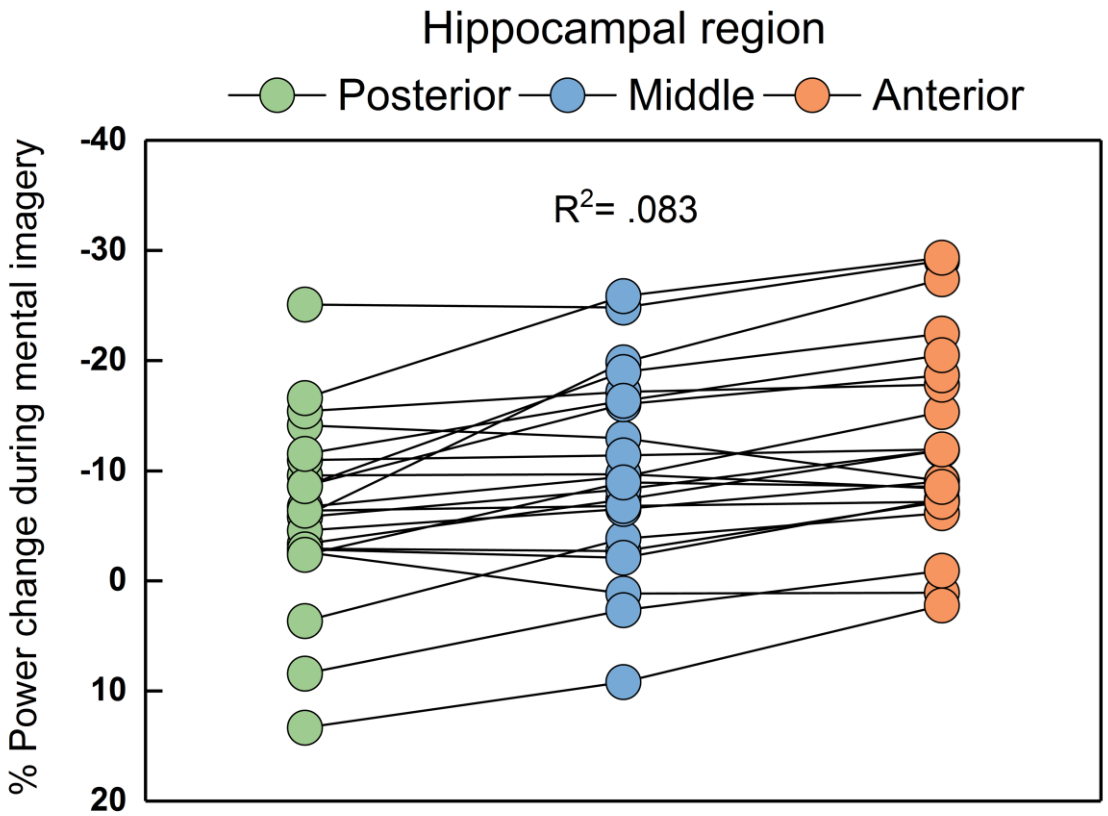

Figure 3. Gradient of theta power change along the hippocampal axis during mental imagery. The magnitude of theta power change increased significantly from posterior to anterior segments. This linear increase along the hippocampal axis was present in 15 of the 22 participants.

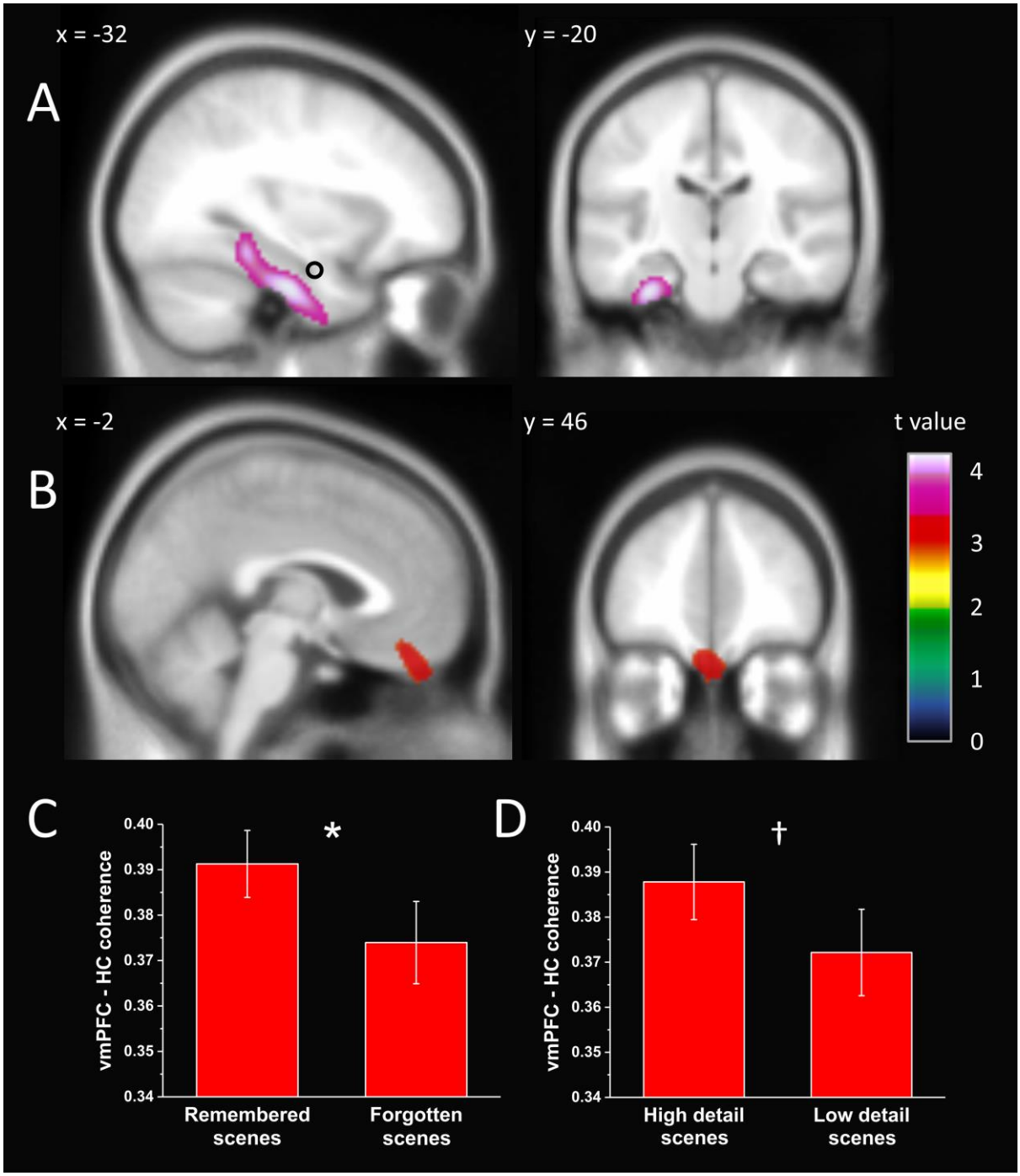

Figure 4. Brain areas displaying higher theta coherence with the left anterior hippocampus during scene imagination compared to object imagination. ***A***, The fusiform and parahippocampal cortices showed higher coherence with the hippocampal source (black circle), display thresholded at $p < 0.001$ uncorrected, superimposed on the MNI 152 T1 image. ***B***, The vmPFC, display thresholded at $p < 0.005$ uncorrected, also showed higher coherence with the hippocampal source (black circle). No areas showed higher theta coherence with the hippocampus for object over scene imagery. ***C***, Coherence between the vmPFC and hippocampus was significantly higher for subsequently remembered than forgotten scenes, *$p = 0.018$. ***D***, A similar trend was observed for scenes imagined in high versus low detail, †$p = 0.058$. Error bars represent ± 1 SEM.

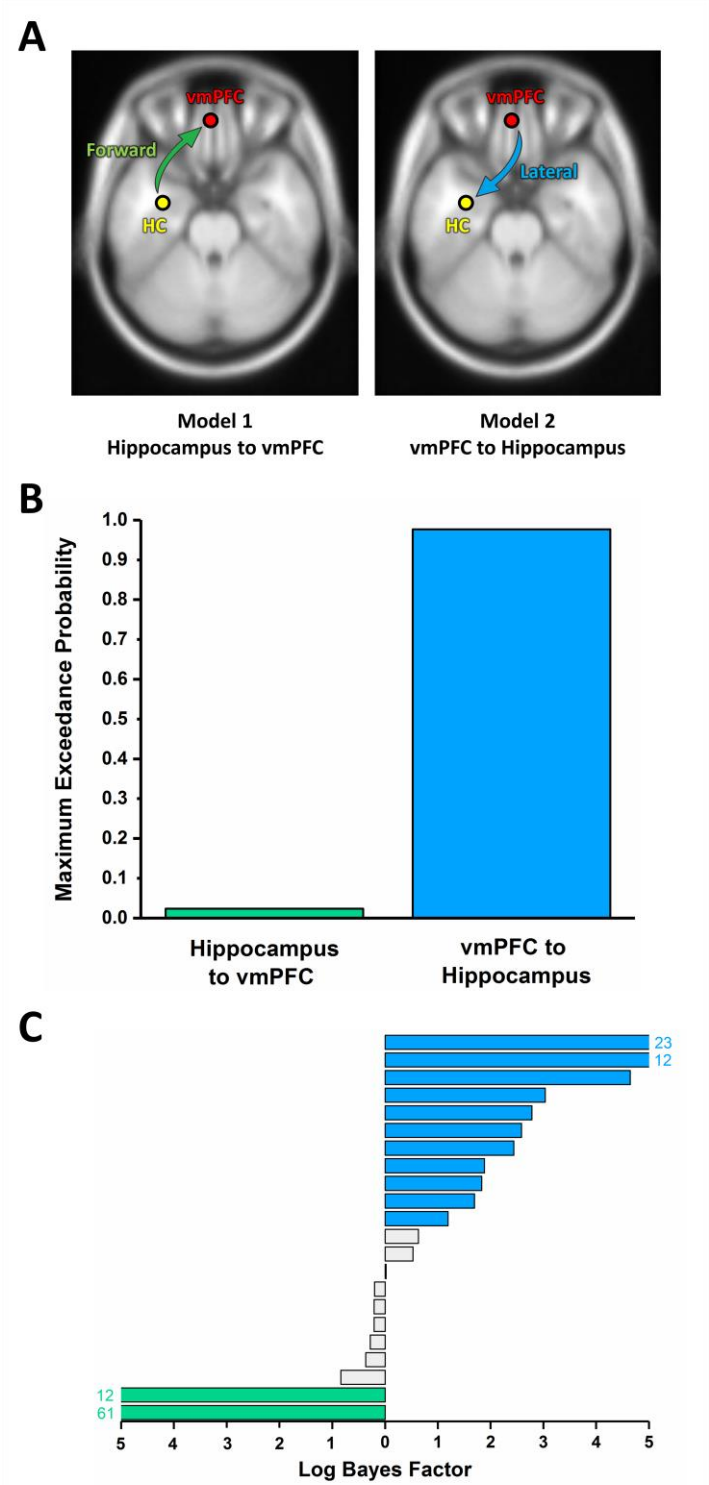

Figure 5. Dynamic Causal Modelling of the interaction between the hippocampus and vmPFC. *A*, Two proposed models of effective connectivity between the coherent peaks in hippocampus and vmPFC. ***B***, Results of Bayesian Model Comparison indicated a stronger influence of the vmPFC on hippocampal activity during scene imagination. ***C***, Log Bayes factors for each participant. Blue bars indicate positive to strong evidence for vmPFC driving hippocampus, the model which most consistently fit across participants. Green bars represent the only two cases where evidence of the hippocampus driving vmPFC was observed. Grey bars represent the remaining participants where there was no conclusive evidence for either model. Where log Bayes factors exceeded five, bars are truncated and the exact values are adjacently displayed.

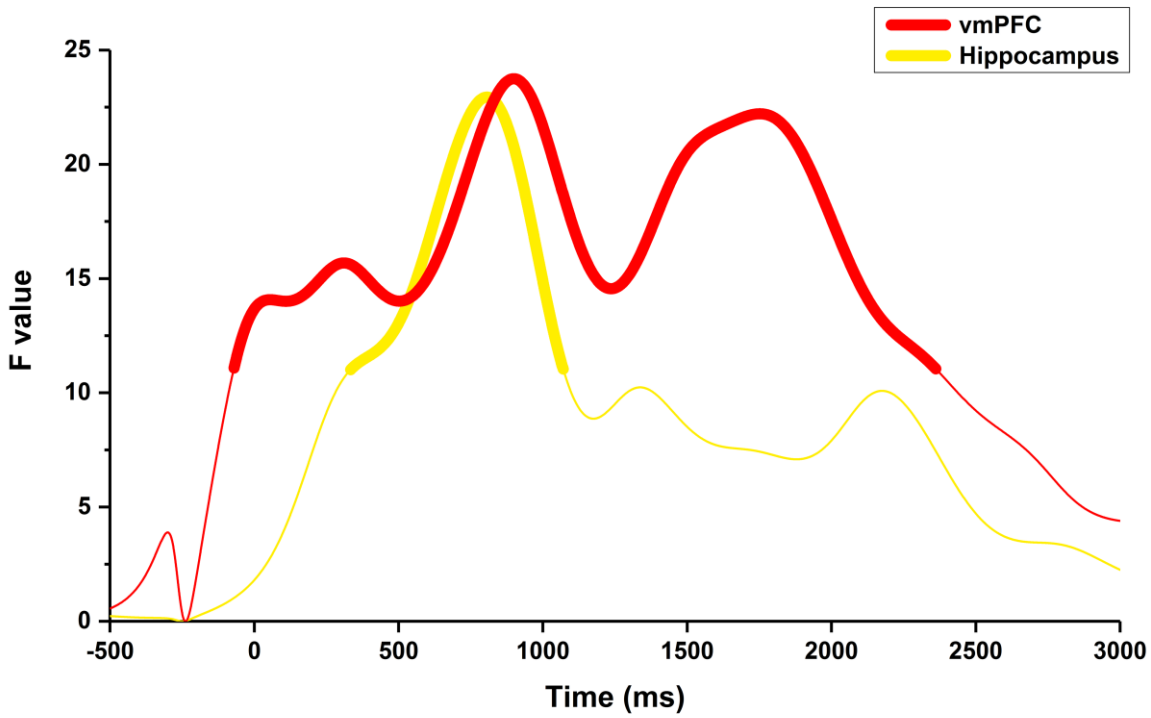

Figure 6. Temporal profile of theta power changes in the vmPFC and hippocampus during scene construction. Line segments in bold indicate periods of significant ($p < 0.05$ FWE corrected) changes in power relative to the pre-imagination period for both the vmPFC (red) and hippocampus (yellow). An initial peak in vmPFC activity was observed 310 milliseconds following cue offset, consistent with a role for the vmPFC in driving hippocampal activity. Maximal activation of both regions occurred within a narrow temporal window (hippocampus: 806 ms, vmPFC: 899 ms). A peak of similar magnitude was evident in the vmPFC at a later stage in the imagination period (1752 ms).

Table 1. Properties of the word stimuli.

Word property		**Word type**			**p-value**	
Lexical criteria	Scene	Object	Number	Scene/Object	Scene/Number	Object/Number
Number of syllables[a]	2.24 (0.87)	2.24 (0.75)	2.24 (0.79)	1	1	1
Number of letters[a]	6.91 (1.95)	6.89 (1.82)	7.03 (2.14)	0.97	0.72	0.68
Number of phonemes[a]	5.83 (1.86)	5.71 (1.64)		0.68		
Number of orthographic neighbours[a]	1.94 (4.16)	2.12 (3.91)		0.81		
Number of phonological neighbours[a]	4.39 (9.76)	4.93 (8.80)		0.72		
Including homophones[a]	4.73 (10.38)	5.16 (9.46)		0.79		
Number of phonographic neighbours[a]	1.01 (2.57)	1.19 (2.65)		0.68		
Including homophones[a]	1.08 (2.84)	1.33 (2.73)		0.58		
Word frequency: Zipf[b]	3.88 (0.70)	3.80 (0.61)		0.46		
Age of acquisition[c]	7.53 (1.98)	7.40 (2.12)		0.70		
Emotional constructs						
Valence[d]	5.79 (1.11)	5.73 (1.07)		0.74		
Number of positive words[d,e]	60 (80%)	62 (83%)		0.86		
Hedonic valence[d,f]	1.15 (0.73)	1.09 (0.69)		0.62		
Arousal[d]	4.16 (0.96)	4.10 (0.95)		0.68		
Imagery						
Concreteness[g]	4.67 (0.19)	4.67 (0.24)		0.87		
Imageability[h]	4.44 (0.26)	4.41 (0.32)		0.57		

Means (standard deviations). Two-tailed p-values for t-tests (χ^2 test for the number of positive words). Note that each comparison was assessed separately in order to provide a greater opportunity for any differences between conditions to be identified.

[a]From the English Lexicon Project (Balota et al. (2007): exlexicon.wustl.edu).

[b]From van Heuven et al. (2014). The Zipf scale is a standardised measure of word frequency using a logarithmic scale. Values go from 1 (low frequency words) to 6 (high frequency words).

[c]From Kuperman et al. (2012).

[d]From Warriner et al. (2013).

[e]Positive words were those that had a valence score greater than or equal to 5.

[f]Hedonic valence is the distance from neutrality (i.e., from 5), regardless of being positive or negative, as per Vigliocco et al. (2014).

[g]From Brysbaert et al. (2014).

[h]From Clark et al. (2018).

Table 2. Scanner trial ratings (mean, SD).

	Condition				p-value
	Scene	Object	Counting	Unsuccessful	Scene/Object/Counting
Proportion of total trials (%)	32.56 (2.51)	31.03 (2.90)	32.28 (1.24)	4.13 (3.10)	0.142
Reclassified trials (%)	As Object	As Scene			Scene/Object
	3.03 (3.01)	5.78 (8.15)			0.110
					Scene/Object
High detail (%)	71.41 (13.79)	74.70 (12.71)			0.199
High concentration (%)			78.09 (7.91)		

Table 3. Post-scan recognition memory performance, d' and c (response bias) values (mean, SD) for scenes and objects.

	Condition		p-value (vs 50% chance)		p-value (Scene vs Object)
	Scene	Object	Scene	Object	
Correct recognition (%)	85.67 (10.17)	88.35 (8.56)	<0.001	<0.001	0.048
d'	2.92 (1.26)	4.02 (1.28)			<0.001
c	0.21 (0.52)	0.70 (0.54)			0.002